



OPEN

# Diffusion of hydrocarbons diluted in supercritical carbon dioxide

Denis Saric<sup>1</sup>, Gabriela Guevara-Carrion<sup>1</sup>, Yury Gaponenko<sup>2</sup>, Valentina Shevtsova<sup>3,4</sup> & Jadran Vrabec<sup>1</sup>✉

Mutual diffusion of six hydrocarbons (methane, ethane, isobutane, benzene, toluene or naphthalene) diluted in supercritical carbon dioxide (CO<sub>2</sub>) is studied by molecular dynamics simulation near the Widom line, i.e., in the temperature range from 290 to 345 K along the isobar 9 MPa. The CO<sub>2</sub> + aromatics mixtures are additionally sampled at 10 and 12 MPa and an experimental database with Fick diffusion coefficient data for those systems is provided. Taylor dispersion experiments of CO<sub>2</sub> with benzene, toluene, n-dodecane and 1,2,3,4-tetrahydronaphthalene are conducted along the  $p = 10$  MPa isobar. Maxwell–Stefan and Fick diffusion coefficients are analyzed, together with the thermodynamic factor that relates them. It is found that the peculiar behavior of the Fick diffusion coefficient of some CO<sub>2</sub> mixtures in the extended critical region is a consequence of the thermodynamic factor minimum due to pronounced clustering on the molecular scale. Further, the strong dependence of the Fick diffusion coefficient on the molecular mass of the solute as well as the breakdown of the Stokes–Einstein relation near the Widom line are confirmed. Eleven correlations for the prediction of the Fick diffusion coefficient of CO<sub>2</sub> mixtures are assessed. An alternative two-step approach for the prediction of the infinite dilution Fick diffusion coefficient of supercritical CO<sub>2</sub> mixtures is proposed. It requires only the state point in terms of temperature and pressure (or density) as well as the molecular solute mass as input parameters. First, entropy scaling is applied to estimate the self-diffusion coefficient of CO<sub>2</sub>. Subsequently, this coefficient is used to determine the infinite dilution Fick diffusion coefficient of the mixture, based on the finding that these two diffusion coefficients exhibit a linear relationship, where the slope depends only on the molecular solute mass.

Carbon dioxide (CO<sub>2</sub>) has unique properties that make it an attractive working fluid for various supercritical fluid (SCF) applications<sup>1</sup>. It consists of small, linear molecules with enhanced diffusivity and has a relatively mild critical point ( $T_c = 304.13$  K,  $p_c = 7.38$  MPa,  $\rho_c = 467.6$  kg/m<sup>3</sup>). Moreover, it is chemically stable, environmentally friendly and effectively absorbs many solute species. Hence, supercritical CO<sub>2</sub> (scCO<sub>2</sub>) can replace water in textile dyeing<sup>2</sup> or serve as an alternative to organic solvents in separation processes<sup>3</sup>.

In practical industrial scenarios, CO<sub>2</sub> often contains impurities, such as traces of hydrocarbons, which can significantly affect the thermophysical behavior of CO<sub>2</sub> mixtures in their extended critical region. Understanding diffusion in CO<sub>2</sub> + hydrocarbon mixtures under supercritical conditions is thus crucial for the development, control and optimization of processes like enhanced oil recovery<sup>4</sup> or CO<sub>2</sub> sequestration<sup>5</sup>. However, mutual diffusion coefficient data of such systems, particularly near the critical point, are scarce<sup>6</sup>. Experimental literature data are primarily limited to the low-temperature, high-density region, resulting in a lack of data for the low-density, high-temperature SCF region. Bridging this gap is essential for emerging SCF processes<sup>7</sup>.

Several semi-empirical correlations of the Stokes–Einstein<sup>8–15</sup> or free-volume type<sup>16–18</sup> have been developed to estimate the Fick diffusion coefficient of CO<sub>2</sub> mixtures. These correlations are simple, but do not rely on a molecular-scale understanding of the underlying diffusion process. Moreover, they often fail to accurately reproduce the Fick diffusion coefficient of scCO<sub>2</sub> mixtures<sup>19,20</sup>, especially near the critical point. For instance, the Stokes–Einstein-type correlations are mainly suited for the liquid-like region<sup>7</sup>, but tend to fail at low density<sup>21</sup>. Therefore, acquiring new data is necessary to critically reassess existing correlations and to develop improved ones<sup>7</sup>.

The lack of mutual diffusion coefficient data for high-pressure CO<sub>2</sub> + hydrocarbon mixtures is in stark contrast to their importance for reservoir processes<sup>20</sup>. The temperature, pressure and composition dependencies of the Fick diffusion coefficient remain largely unexplored over a wide range of thermodynamic conditions<sup>22</sup>.

<sup>1</sup>Thermodynamics, Technical University of Berlin, Ernst-Reuter-Platz 1, 10587 Berlin, Germany. <sup>2</sup>MRC, CP-165/62, Université libre de Bruxelles (ULB), Ave. F.D. Roosevelt 50, B-1050 Brussels, Belgium. <sup>3</sup>Fluid Mechanics Group, Faculty of Engineering, Mondragon University, 20500 Mondragon, Spain. <sup>4</sup>IKERBASQUE, Basque Foundation for Science, Plaza Euskadi 5, 48009 Bilbao, Spain. ✉email: vrabec@tu-berlin.de

Experimental studies on CO<sub>2</sub> mixtures with benzene<sup>12,18,23–32</sup>, toluene<sup>5,13,25,26, 32,33</sup> or naphthalene<sup>12,18,34–41</sup> at high pressure (see Table 1) have provided valuable insights into the Fick diffusion coefficient, revealing a peculiar behavior in certain near-critical regions<sup>28,30,42</sup>, a significant dependence on the molecular mass of the solute<sup>7,14,24,43</sup> and deviations from the conventional Stokes–Einstein behavior<sup>7,22,31,44–46</sup>.

In the extended critical region, a slight increase of temperature along a supercritical isobar may substantially reduce the density and shear viscosity, while it rises the intra-diffusion coefficients of the mixture's components<sup>47</sup>. In that region, SCF can exhibit liquid-like (high density, high viscosity and low diffusivity) or gas-like (low density, low viscosity and high diffusivity) characteristics<sup>47–51</sup>. These regions are demarcated by the so-called Widom line, which can be considered as an extension of the vapor pressure curve up to approximately  $10 \cdot p_c$ <sup>52</sup>. Close to the Widom line pronounced density fluctuations occur<sup>53–55</sup>, leading to a strongly non-ideal behavior of the mixture<sup>56,57</sup> and large changes of its thermodynamic and transport properties<sup>47,58–60</sup>. One well-known example is the isobaric heat capacity, which exhibits a peak at the Widom line that gradually fades with increasing pressure<sup>47,61</sup>.

This work seeks to contribute to the understanding of the diffusion behavior of binary CO<sub>2</sub> mixtures containing hydrocarbons in the extended critical region. To cover a broad range of solute size, methane, ethane, isobutane, benzene, toluene and naphthalene are considered in a systematic way. Building upon our recent work on thermodynamics, dynamics and structure of scCO<sub>2</sub> mixtures across the Widom line<sup>47</sup>, it focuses on the

Authors	Year	$N_p$	$T / K$	$p / MPa$	Experimental method
CO <sub>2</sub> + Benzene					
Swaid and Schneider <sup>23</sup>	1979	22	313.15–328.15	11–15	TD
Sassiat et al. <sup>12</sup>	1987	11	303.15–333.15	11–26	TD
Uwezava and Nagashima <sup>24</sup>	1992	5	299.15–308.15	9–10.5	TD
Funazukuri et al. <sup>18</sup>	1992	2	313.2	16–25	TD
Levelt Sengers et al. <sup>25</sup>	1993	9	306.8–314.4	9.7–13.5	TD
Suarez et al. <sup>26</sup>	1993	15	313.15–333.15	15–35	TD
Funazukuri and Nishimoto <sup>27</sup>	1996	31	313.2	8.5–30	TD
Funazukuri et al. <sup>28</sup>	2001	176	308.15–328.15	6–30	TD
Filho et al. <sup>29</sup>	2002	7	313.15–333.15	12–16	TD
Nishiumi and Kubota <sup>30</sup>	2007	94	313.15	2.2–16.7	TD
Lin et al. <sup>31</sup>	2010	36	313.15–373.15	10–30	TD
Santos et al. <sup>32</sup>	2022	7	306.15–320.15	7.5–17.5	TD
This work	2023	7	302.8–341.5	10	TD
CO <sub>2</sub> + Toluene					
Bruno <sup>33</sup>	1989	6	313	13.3–30.4	SFC
Levelt Sengers et al. <sup>25</sup>	1993	8	306.8–314.4	9.7–13.5	TD
Suarez et al. <sup>26</sup>	1993	15	313.15–333.15	15–35	TD
Lai and Tan <sup>13</sup>	1995	18	308–328	7.5–14.3	CCC
Cadogan <sup>5</sup>	2015	30	298–423	1–68	TD
Lin et al. <sup>31</sup>	2010	36	313.15–373.15	10–30	TD
Santos et al. <sup>32</sup>	2022	12	306.15–320.15	7.5–17.5	TD
This work	2023	8	302.9–341.5	10	TD
CO <sub>2</sub> + Naphthalene					
Knaff and Schlünder <sup>34</sup>	1987	16	308.15–333.15	11.8–22.6	PSSDT
Sassiat et al. <sup>12</sup>	1987	11	303.15–333.15	11–26	TD
Lamb et al. <sup>35</sup>	1989	25	351.15	2–20	NMR-Bessel
Funazukuri et al. <sup>18</sup>	1992	2	313.2	16–25	TD
Akgerman et al. <sup>36</sup>	1996	17	308–328	9.6–24.9	TD
Klask <sup>37</sup>	1998	46	309–330.7	8.9–20	PSSDT
Higashi et al. <sup>38</sup>	1998	15	308.2	7.2–15.2	PSSDT
Higashi et al. <sup>39</sup>	1999	35	308.2–318.2	7.7–20	PSSDT
Higashi et al. <sup>40</sup>	2002	7	308.2	8.2–10.4	PSSDT
Kong et al. <sup>41</sup>	2011	42	308.15 and 333.15	7–40	TD

**Table 1.** Experimental literature data for CO<sub>2</sub> mixtures with benzene, toluene or naphthalene at different temperatures and pressures. The number of data points is given by  $N_p$ . The accompanying numerical data are provided in the Supplementary Information. The abbreviations for the experimental methods are TD, Taylor dispersion; SFC, Supercritical fluid chromatography; CCC, Coated capillary column, PSSDT, Pseudo-steady state solid dissolution technique and NMR-Bessel, NMR fixed field gradient spin-echo Bessel function analysis technique.

thermodynamic factor and diffusion coefficients. For this purpose, equilibrium molecular dynamics simulations were conducted to sample intra-diffusion, Maxwell–Stefan and Fick diffusion coefficients of those scCO<sub>2</sub> mixtures. The self-diffusion coefficients of the components within a mixture are commonly referred to as intra-diffusion coefficients, which helps to distinguish them from the self-diffusion coefficient of pure substances. Whenever possible, simulation data are compared with experiments and equation of state (EoS) models. An overview of the different diffusion coefficient types addressed in this work is given in Table 2. Further, new experimental data for CO<sub>2</sub> mixtures with benzene, toluene, n-dodecane and 1,2,3,4-tetrahydronaphthalene (THN) at high temperatures along the isobar  $p = 10$  MPa are presented, cf. Table 3.

Molecular modeling and simulation is recognized as a powerful tool for predicting thermodynamic properties of CO<sub>2</sub> mixtures<sup>62</sup>. It provides valuable insights into the molecular-level interactions, structure and dynamics of fluids. For instance, such simulation studies have revealed significant clustering<sup>63,64</sup> and the breakdown of the Stokes–Einstein relation in the vicinity of the Widom line<sup>65,66</sup>. However, conducting molecular simulations in the extended critical region poses challenges due to strong density fluctuations<sup>55</sup>, requiring a significant sampling effort to obtain statistically reliable results. Hence, only few molecular dynamics simulation studies have investigated diffusion coefficients of CO<sub>2</sub> mixtures with methane<sup>56,67–70</sup>, ethane<sup>68</sup>, benzene<sup>71–74</sup>, toluene<sup>72,73</sup> or naphthalene<sup>73–78</sup> at near-critical and/or supercritical states.

In this work, the Fick diffusion coefficient of scCO<sub>2</sub> mixtures with benzene, toluene, n-dodecane and THN at  $p = 10$  MPa was determined experimentally with the Taylor dispersion technique. This approach relies on the diffusive spreading of a small volume of a solution injected into a laminar stream of a carrier fluid. Axial dispersion spreads out the solute pulse longitudinally, while radial diffusion confines the pulse. Upon the flow of the mixture through a long capillary, a Gaussian concentration distribution, known as Taylor peak, is formed as a result of the combined effects of convective flow and molecular diffusion. Subsequently, the concentration distribution is detected at the end of the capillary. The Taylor dispersion technique has been employed since 1979<sup>23</sup>, but its accuracy still requires improvement for supercritical mixtures<sup>79</sup>. For instance, the solute is injected as a pure fluid into the CO<sub>2</sub> carrier, such that the diffusion process undergoes the entire composition range until it asymptotically reaches infinite dilution.

## Results

Mass transport in mixtures is commonly described by Fick’s “law”, which correlates the molar flux to the mole fraction gradient via the Fick diffusion coefficient. However, the actual thermodynamic driving force behind mass transport is the chemical potential gradient, which is balanced by friction forces between the mixture’s components as embodied by Maxwell–Stefan theory. This theory treats kinetics and thermodynamics separately, wherein the latter is given by the so-called thermodynamic factor  $\Gamma^{80}$ . The kinetic contribution is considered by the Maxwell–Stefan diffusion coefficient  $\mathfrak{D}$ , which can be obtained from the phenomenological Onsager coefficients by molecular dynamics simulation. The Fick diffusion coefficient  $D$  can be determined experimentally.

Symbol	Name
$D_{\text{CO}_2}$	Self-diffusion coefficient of pure CO <sub>2</sub>
$D_{\text{CO}_2}^+$	Scaled self-diffusion coefficient of pure CO <sub>2</sub>
$D_i$	Intra-diffusion coefficient of component $i$ in a mixture
$\mathfrak{D}$	Maxwell–Stefan diffusion coefficient
$D$	Fick diffusion coefficient
$D^{x_i \rightarrow 1}$	Infinite dilution Fick diffusion coefficient

**Table 2.** Overview of the diffusion coefficient types addressed in this work.

CO <sub>2</sub> + Benzene		CO <sub>2</sub> + Toluene		CO <sub>2</sub> + n-Dodecane		CO <sub>2</sub> + THN	
$T / \text{K}$	$D / 10^{-8} \text{ m}^2 \text{ s}^{-1}$	$T / \text{K}$	$D / 10^{-8} \text{ m}^2 \text{ s}^{-1}$	$T / \text{K}$	$D / 10^{-8} \text{ m}^2 \text{ s}^{-1}$	$T / \text{K}$	$D / 10^{-8} \text{ m}^2 \text{ s}^{-1}$
302.9	1.159 (20)	303.0	1.053 (33)	303.0	0.915 (92)	303.0	0.896 (58)
312.6	1.606 (39)	307.8	1.294 (13)	307.8	0.965 (13)	307.7	1.028 (21)
317.3	1.915 (44)	310.2	1.397 (19)	310.2	1.015 (44)	310.1	1.001 (22)
322.3	1.969 (81)	312.7	1.562 (51)	312.5	1.210 (30)	312.6	1.122 (51)
331.9	2.868 (134)	317.3	1.807 (61)	317.4	1.388 (105)	317.5	1.367 (24)
336.8	3.197 (170)	322.3	1.910 (123)	322.3	1.611 (123)	322.2	1.502 (57)
341.6	3.493 (160)	332.0	2.636 (118)	327.1	1.758 (96)	327.0	1.593 (93)
		341.5	3.111 (127)	331.9	1.659 (39)	331.8	1.142 (114)
				336.7	1.548 (192)	336.7	0.933 (41)
				341.5	1.436 (201)	341.5	0.871 (106)

**Table 3.** Present experimental data for CO<sub>2</sub> mixtures with benzene, toluene, n-dodecane and THN along the isobar  $p = 10$  MPa. The numbers in parentheses indicate the uncertainties in last digits.

The ratio between these two diffusion coefficients is the thermodynamic factor,  $\Gamma = D/\mathcal{D}$ , which cannot be directly accessed with experiments.

In this study, six binary CO<sub>2</sub> mixtures were investigated close to the infinite dilution limit (typically with 0.5, 1.0 and 1.5 mol% of the solute) by molecular simulation. The extended critical region was in the focus, i.e., temperatures from 290 to 345 K along the isobar  $p = 9$  MPa, and for CO<sub>2</sub> mixtures with the aromatics, additionally the isobars  $p = 10$  and 12 MPa were considered. Taylor dispersion experiments of scCO<sub>2</sub> mixtures with benzene, toluene, n-dodecane and THN were also conducted at  $p = 10$  MPa. Within the extended critical region, it was found that the thermodynamic factor, and consequently the Fick diffusion coefficient, exhibit a peculiar behavior.

### Thermodynamic factor

The thermodynamic factor  $\Gamma = (\partial\mu_1/\partial x_1)_{T,p} \cdot x_1/(RT)$ , being the partial derivative of the chemical potential  $\mu_1$  with respect to the mole fraction  $x_1$ , accounts for the non-ideality and is unity for ideal mixtures according to Raoult. Its dependence on temperature  $T$  and pressure  $p$  is exemplarily depicted for scCO<sub>2</sub> mixtures with 0.5 mol% of benzene or naphthalene in Fig. 1 (top). Plots on the temperature, pressure and mole fraction dependencies of  $\Gamma$  for the remaining mixtures are given in Figs. S1 to S4 of the Supplementary Information (SI).

The thermodynamic factor, calculated by both Kirkwood-Buff integration and EoS, exhibits a consistent qualitative pattern characterized by an often pronounced minimum near the Widom line<sup>57</sup>. For example, the thermodynamic factor of scCO<sub>2</sub> containing only 0.5 mol% of naphthalene, reaches a value as low as  $\Gamma = 0.45$  at  $T = 320$  K along the isobar  $p = 9$  MPa, cf. Fig. S1. Note that the magnitude of its minimum varies with the solute. In fact, as the size difference between the solvent and solute increases, the minimum becomes deeper, which aligns with the expected increase of the mixtures' non-ideality.

In general, molecular simulation data sampled with Kirkwood-Buff integration tend to overestimate the thermodynamic factor when compared to the values obtained from EoS<sup>81</sup>. As the solute mole fraction goes to zero,  $\Gamma \rightarrow 1$ , cf. Figs. S1 to S4. Further, the thermodynamic factor minimum at a given mixture composition fades with rising pressure and shifts to higher temperatures, cf. Fig. 1.

The presence of that minimum is attributed to the proximity of such states to the critical point, where  $\Gamma = 0$ <sup>82</sup>. In fact, the observed strong sensitivity of the thermodynamic factor to even small changes of solute concentration<sup>30</sup> and the occurrence of clustering<sup>63</sup> can be related to this proximity. The extent of clustering can be quantified by the excess number of solvent molecules around a given solute molecule, relative to a uniform bulk density distribution<sup>47,64</sup>. Consequently, the presence of clustering may result in a negative partial molar volume of the solute component near the infinite dilution<sup>47</sup>.

Fig. 1 (bottom) illustrates the dependence of the excess coordination number on temperature and pressure for scCO<sub>2</sub> mixtures with benzene and naphthalene along the isobars  $p = 10$  and 12 MPa. The temperature where thermodynamic non-idealities are most significant, indicated by the minimum of  $\Gamma$ , approximately coincides with the one where the largest number of solvent molecules gathers around a given solute molecule. This suggests that clustering on the molecular scale is responsible for the observed non-idealities.

### Fick diffusion coefficient

The Maxwell–Stefan and intra-diffusion coefficients were sampled with molecular dynamics simulation at three solute mole fractions (typically 0.5, 1.0 and 1.5 mol%) in the regarded temperature and pressure range. Using

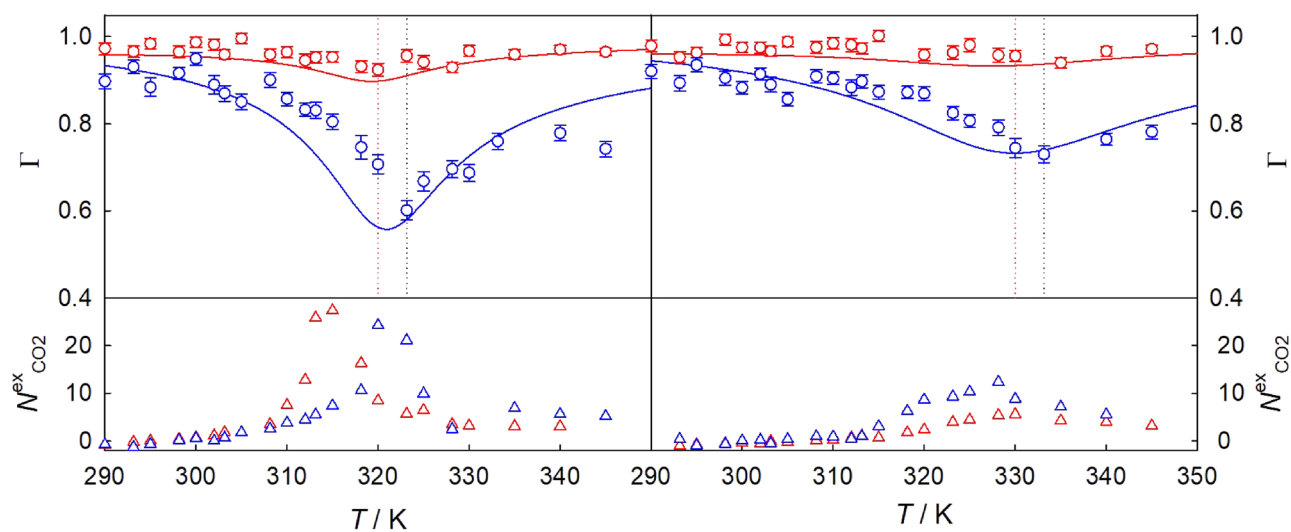


**Figure 1.** Temperature dependence of the thermodynamic factor (top) and the excess number of solvent molecules (bottom) of CO<sub>2</sub> mixtures with 0.5 mol% of benzene (red) or naphthalene (blue) along the isobars  $p = 10$  MPa (left) and 12 MPa (right). Symbols represent molecular simulation data along the isobars  $p = 10$  and 12 MPa, respectively. Solid lines depict the thermodynamic factor calculated with TRENDS 5.0<sup>83</sup> on the basis of the Peng–Robinson EoS for CO<sub>2</sub> + benzene ( $k_{12} = 0.0967$ )<sup>84</sup> or CO<sub>2</sub> + naphthalene ( $k_{12} = 0.016, l_{12} = -0.173$ )<sup>40</sup>. Dotted lines indicate the thermodynamic factor minimum inferred from molecular simulation data.

Kirkwood-Buff integration simulation data for the thermodynamic factor, the Fick diffusion coefficient was obtained from  $D = \bar{D} \cdot \Gamma$ . In the infinite dilution limit, Fick and Maxwell–Stefan diffusion coefficients coincide, thus both can be estimated by the extrapolation of the intra-diffusion coefficient of the solute (2) to the limit where it is infinitely diluted in CO<sub>2</sub> solvent (1)<sup>56,85</sup>. This extrapolation of the intra-diffusion coefficient is associated with lower statistical uncertainties than the directly sampled Maxwell–Stefan diffusion coefficient, since the latter is a collective property.

The influence of solute mole fraction on the Maxwell–Stefan diffusion coefficient was found to be weak, as illustrated in Fig. 2 or Fig. S5. In contrast, the Fick diffusion coefficient depends significantly on composition in the critical region, which can be attributed to substantial changes of the thermodynamic factor. Usually, both the Maxwell–Stefan and Fick diffusion coefficients increase with rising temperature. However, the Fick diffusion coefficient may decrease near the Widom line as the temperature rises due to a significant reduction of the thermodynamic factor.

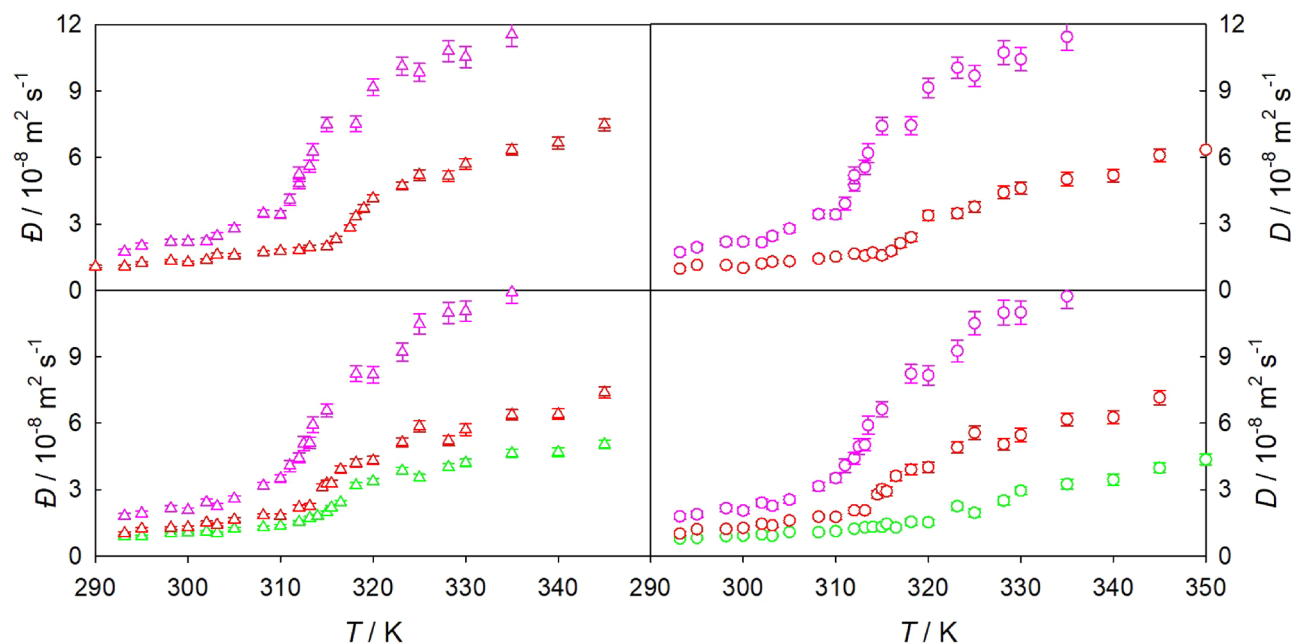


**Figure 2.** Temperature dependence of the Maxwell–Stefan (left) and Fick diffusion (right) coefficients of CO<sub>2</sub> mixtures with 0.5 mol% (bottom) and 1.5 mol% (top) of ethane (pink), benzene (red) or naphthalene (green) along the isobar  $p = 9$  MPa. Symbols represent molecular simulation data.

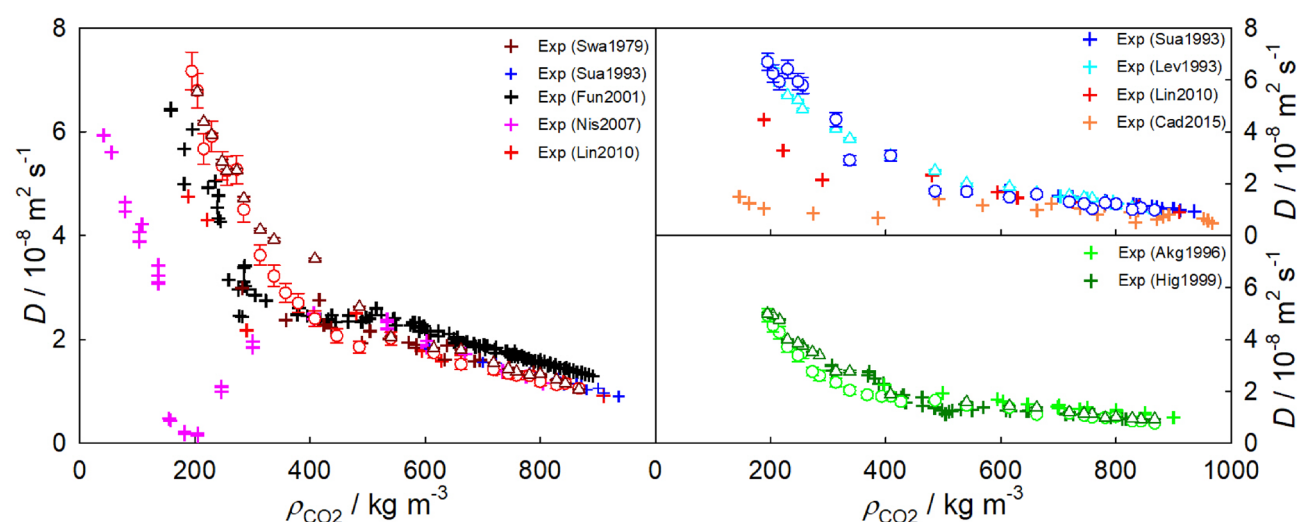


**Figure 3.** Density dependence of the Fick diffusion coefficient of CO<sub>2</sub> mixtures with benzene (left), toluene (top right) or naphthalene (bottom right). Open circles represent molecular simulation data for a solute mole fraction of 1.0 mol% for benzene or toluene and of 0.3 mol% for naphthalene. Open triangles represent the infinite dilution Fick diffusion coefficient along the isobar  $p = 9$  MPa. Experimental data for benzene<sup>23,26,28,30,31</sup> at  $p = 2.2$  to 35 MPa, toluene<sup>5,25,26,31</sup> at  $p = 1$  to 68 MPa and naphthalene<sup>36,39</sup> at  $p = 2$  to 40 MPa are depicted by crosses. Further experimental data are listed in Table 1, but were left out in the plot to avoid visual clutter.

### Density dependence

The density dependence of the Fick diffusion coefficient of CO<sub>2</sub> mixtures with the aromatics benzene, toluene or naphthalene is shown in Fig. 3. To facilitate a more straightforward comparison of data from different sources, present simulation results were compared to experimental data of mixtures having the same density, but may have been measured at different temperatures or pressures, cf. Table 1.

In general, a good qualitative agreement between experimental literature and present simulation data is found. However, it is evident that the experimental data scatter significantly at near-critical densities. As expected, the Fick diffusion coefficient gradually rises with decreasing density, but the presence of a peculiar behavior of that coefficient close to the Widom line can be inferred. For instance, either the Fick diffusion coefficient exhibits a minimum (red crosses in Fig. 3) or the rate of its decrease with rising density is slowed down in certain state regions (black crosses in Fig. 3). This is confirmed by present experiments and is most pronounced for large and heavy solutes, such as n-dodecane or THN, which show a stronger drop of the Fick diffusion coefficient in the vicinity of the Widom line than benzene or toluene, cf. Table 3. These experimental findings can be attributed to a stronger departure from ideality of the mixture, leading to a more pronounced thermodynamic factor minimum<sup>30</sup>. In contrast to molecular simulation runs, the exact solute mole fraction is unknown in most diffusion coefficient experiments. An exception are the Fick diffusion coefficient data for CO<sub>2</sub> + benzene from Nishiumi und Kubota<sup>30</sup>, which were measured at a solute mole fraction of approximately 1.7 mol%<sup>86</sup>.

The quantitative agreement between data from experiment and simulation is good at high densities and low temperatures along the isobar  $p = 9$  MPa. The peculiar behavior of the experimentally determined Fick diffusion coefficient is qualitatively replicated by simulation data at finite mole fractions. The thermodynamic factor has a minimum close to the Widom line, and consequently decreases the Fick diffusion coefficient in the near-critical region. This strong concentration dependence of that coefficient<sup>87</sup> and its peculiar behavior fade in the infinite dilution limit, where the thermodynamic factor converges to unity. Hence, the thermodynamic factor is a key property to rationalize diffusion in SCF mixtures. In fact, the thermodynamic factor has been demonstrated to cause the strong reduction of the experimental Fick diffusion coefficient of CO<sub>2</sub> + naphthalene even for a solute mole fraction as low as 0.1 mol%<sup>40,86</sup>.

The strong variations of density and thus of the diffusion coefficients are most pronounced at the lowest isobar  $p = 9$  MPa, where the mixtures are closer to the critical point of CO<sub>2</sub>. As the pressure increases, the peculiar behavior of both the thermodynamic and transport properties fades<sup>47</sup>. Further, the infinite dilution Fick diffusion coefficient decreases at constant temperature with rising pressure.

A comparison of present experimental data with simulation data for scCO<sub>2</sub> mixtures with benzene or toluene at  $p = 10$  MPa is given in Fig. 4. There, molecular simulation overestimates the experimental Fick diffusion coefficient at low densities for both mixtures, but the qualitative agreement is good. The peculiar behavior of the Fick diffusion coefficient in the near-critical region is both qualitatively and quantitatively replicated at finite mole fractions.

### Solute mass dependence

Previous experimental studies have demonstrated that the infinite dilution Fick diffusion coefficient of 44 scCO<sub>2</sub> mixtures is logarithmically correlated with the mass of the solute<sup>14,43,88</sup>. This suggests that the molecular weight

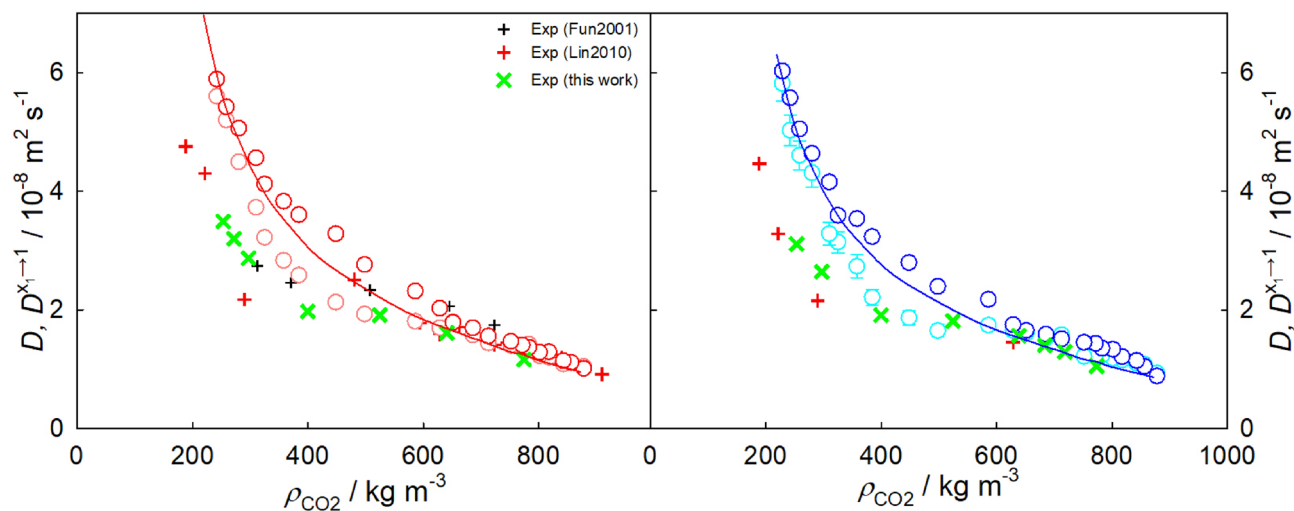


**Figure 4.** Density dependence of the Fick diffusion coefficient of CO<sub>2</sub> mixtures with benzene (left) or toluene (right) along the isobar  $p = 10$  MPa. Circles represent molecular simulation data at a solute mole fraction of 1.5 mol% for benzene (pink) or toluene (cyan). The infinite dilution Fick diffusion coefficient  $D^{x_1 \rightarrow 1}$  of CO<sub>2</sub> + benzene and CO<sub>2</sub> + toluene is depicted by red and blue circles, respectively. Experimental data from this work are shown by green crosses, whereas literature data are represented by black<sup>28</sup> and red<sup>31</sup> plus signs. Solid lines show the predictive approach proposed in this work (Eqs. (2) and (4)). Additional experimental data are listed in Table 1, but were left out of the plot to avoid visual clutter.

of the solute may have a greater impact on mutual diffusion in diluted scCO<sub>2</sub> mixtures than the molecular interactions<sup>14</sup>.

In the present study, the dependence of the infinite dilution Fick diffusion coefficient on molecular solute mass was investigated for six hydrocarbons infinitely diluted in scCO<sub>2</sub> at 22 thermodynamic state points along the isobar  $p = 9$  MPa, cf. Fig. 5. The simulation results validate the trends observed in previous experimental studies. For all mixtures, the infinite dilution Fick diffusion coefficient increases with rising temperature. The slope of that function is consistent within the high-density, liquid-like ( $T < 308.15$  K, dotted lines) and the low-density, gas-like ( $T > 315$  K, dashed lines) SCF regions. At the limits of the regarded temperature range, the curves exhibit a noticeable parallelism, which weakens as the Widom line is approached. In fact, there is a notable 27% change in slope between both density regions when crossing the Widom line of pure CO<sub>2</sub>, i.e. from  $\sim M_2^{-0.528}$  at  $T = 308.15$  K to  $\sim M_2^{-0.719}$  at  $T = 315$  K. Thus, the solute mass dependence of the infinite dilution Fick diffusion coefficient varies significantly across distinct density regions of supercritical fluids.

### Breakdown of Stokes–Einstein relation

The Stokes–Einstein (SE) relation establishes a connection between the diffusive motion of a solute with its size and the surrounding fluid's viscosity. In this work, the SE equation  $D_i = k_B T / (C \eta r_{H,i})$  was applied to the intra-diffusion coefficients of the mixtures' components  $D_i$ . Therein,  $r_{H,i}$  is the hydrodynamic radius of component  $i$ ,  $\eta$  is the shear viscosity of the fluid,  $k_B$  is the Boltzmann constant and  $C$  accounts for the boundary conditions. For slip conditions,  $C = 4\pi$ , whereas for stick conditions,  $C = 6\pi$ . This relation assumes that the hydrodynamic radius  $r_{H,i}$  is constant and independent of temperature<sup>89</sup>, which implies that  $D_i \eta / T$  is temperature-independent<sup>65</sup>.

Several experimental studies have indicated that diffusion in scCO<sub>2</sub> mixtures closely follows the hydrodynamic behavior expected from the SE relation, i.e.  $D_i \propto T/\eta$ <sup>31,44,45</sup>, but its validity was questioned ever since<sup>66,90–92</sup>. The region near the Widom line, where a transition from a high-density to a low-density fluid and a sharp growth of molecule clusters occur, has been found to be correlated to the strong decoupling of diffusion and viscosity, i.e. the breakdown of the SE relation, e.g., for water<sup>65</sup>.

There are different methods to verify the validity of the SE relation<sup>93–95</sup>. One popular approach involves the calculation of the hydrodynamic radius  $r_{H,i}$ , but this requires the knowledge of the boundary conditions and shear viscosity. To avoid issues related to the accuracy of these values, the ratio

$$\frac{D_2}{D_1} = \frac{k_B T / (r_{H,2} \eta C)}{k_B T / (r_{H,1} \eta C)} = \frac{r_{H,1}}{r_{H,2}}, \quad (1)$$

can be considered, where  $D_2$  and  $D_1$  are the intra-diffusion coefficients of the solute and CO<sub>2</sub>, respectively.

The ratio of intra-diffusion coefficients of scCO<sub>2</sub> mixtures along the isobar  $p = 9$  MPa is shown in Fig. 6. As expected from the SE relation, the ratio of hydrodynamic radii remains relatively constant in the high-density, liquid-like region up to the Widom line. There, a significant change of this ratio is observed for several of the studied mixtures, which suggests a breakdown of the SE relation. At higher temperatures, in the low-density, gas-like region, the ratio again follows the expected SE behavior to some extent. It should be noted that the magnitude of the SE breakdown increases with the depth of the thermodynamic factor minimum, thus being related to the non-ideality. A rising pressure weakens this breakdown due to the reduction of fluctuations and clustering related to the critical region<sup>90</sup>. The breakdown of the SE relation implies a change of the predominant diffusion mechanisms around the Widom line, which is associated with an increase of the translational jump-diffusion

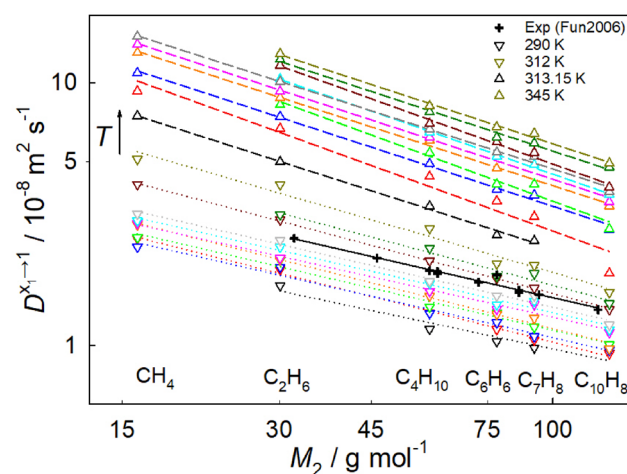


**Figure 5.** Molecular solute mass dependence of the infinite dilution Fick diffusion coefficient of CO<sub>2</sub> mixtures with methane, ethane, isobutane, benzene, toluene or naphthalene. Symbols represent molecular simulation data for different temperatures along the isobar  $p = 9$  MPa: triangles down for  $T = 290$  to  $312$  K and triangles up for  $T = 313.15$  to  $345$  K. Crosses represent experimental literature data<sup>43</sup> for other solutes (ranging from methanol to benzoic acid) in scCO<sub>2</sub> at  $T = 313.2$  K and  $p = 11$  MPa. Dotted and dashed lines represent the liquid- and gas-like regions of pure CO<sub>2</sub>, respectively, which are linear regressions of the form  $\log(D^{x_1 \rightarrow 1}) \sim \log(M_2)$ .

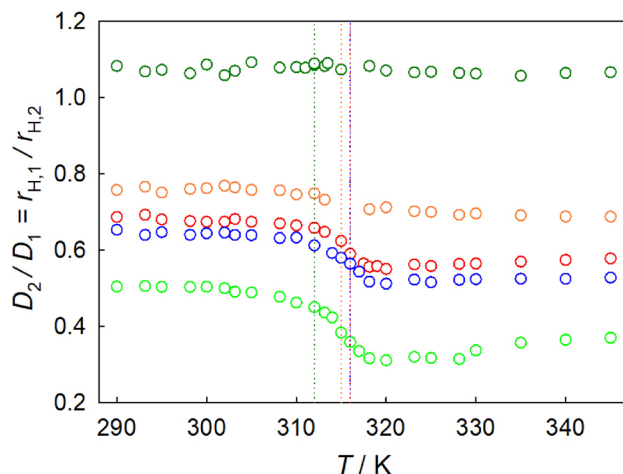


**Figure 6.** Ratio of solute  $D_2$  to solvent  $D_1$  intra-diffusion coefficients of  $\text{CO}_2$  mixtures with 1.5 mol% of ethane (dark green), isobutane (orange), benzene (red), toluene (blue) or with 0.6 mol% of naphthalene (green). Symbols represent simulation data along the isobar  $p = 9$  MPa. Dotted lines indicate the Widom line temperature of the respective  $\text{CO}_2$  mixture inferred from molecular simulation data.

of molecules with large-amplitude displacements. This phenomenon has been observed in aqueous alcoholic mixtures<sup>91,96</sup>.

However, the breakdown of the SE relation is much weaker for  $\text{CO}_2$  + isobutane and may hardly be discerned for  $\text{CO}_2$  + ethane. This can be explained with significantly less pronounced clustering, which is associated with a much weaker non-ideality of those mixtures, due to the relative similarity of these molecular species in comparison to  $\text{CO}_2$  + aromatics<sup>47</sup>.

### Semi-empirical correlations

Eleven correlations for the estimation of the infinite dilution Fick diffusion coefficient of  $\text{scCO}_2$  mixtures as listed in Table S1 were assessed. These correlations include the SE-based equations by Wilke and Chang<sup>8</sup>, Scheibel<sup>9</sup>, Tyn and Calus<sup>10</sup>, Hayduk and Minhas<sup>11</sup>, Sassiat<sup>12</sup>, Lai and Tan<sup>13</sup>, the hydrodynamic equation (modified SE)<sup>14,31</sup> and the modified Rice-Gray correlation<sup>15</sup>, as well as the free-volume based equations by Catchpole and King<sup>16</sup>, He and Yu<sup>17</sup> and Funazukuri and Wakao<sup>97</sup>.

This set of correlations was compared to simulation data for all studied thermodynamic conditions, cf. Fig. 7 and Figs. S6 to S10 of the SI. The average absolute relative deviation (AARD) between these correlations and present simulation data is listed in Table S1 of the SI. Overall, simulation data exhibit a good qualitative agreement with the correlations. The Wilke–Chang and Catchpole–King equations demonstrate the best overall quantitative agreement for the studied  $\text{CO}_2$  + hydrocarbon mixtures, with an AARD of 13.0% and 13.3%, respectively. Although the modified Rice-Gray correlation<sup>15</sup> has a more complex form, it deviates on average by 8.3% from

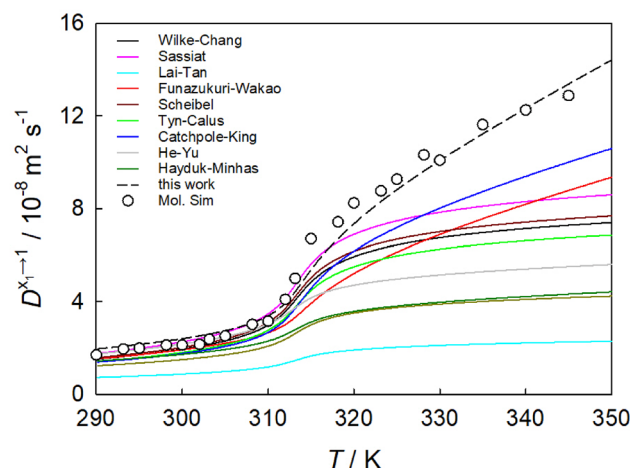


**Figure 7.** Temperature dependence of the infinite dilution Fick diffusion coefficient of  $\text{CO}_2$  + ethane along the isobar  $p = 9$  MPa. Circles represent molecular simulation data obtained from the extrapolation of the intra-diffusion coefficient of ethane to the infinite dilution limit. Solid lines depict semi-empirical correlations<sup>8–14,16–18</sup> and the dashed line shows the present predictive approach introduced later in the manuscript (Eqs. (2) and (4)).

simulation data, compared to the 7.7% and 8.4% of the Wilke–Chang and Tyn–Calus correlations, respectively, for the mixtures of CO<sub>2</sub> with aromatics at all considered pressures. On the other hand, the He–Yu equation<sup>17</sup> is very effective at temperatures below the Widom line, i.e., in the liquid-like SCF, with a deviation of only 6.1% from the simulation data in that region.

At temperatures above the Widom line, i.e., in the gas-like SCF state, the agreement between simulation and the correlations deteriorates significantly. None of the correlations accurately predicts the sampled Fick diffusion coefficient data across the entire range of supercritical conditions. This observation holds also when comparing the correlations with the experimental data from this work for CO<sub>2</sub> mixtures with benzene or toluene at a pressure of 10 MPa. Most correlations show an AARD of at least 20% from present experimental data, cf. Table S1. Exceptions are the correlations by Funazukuri–Wakao<sup>18</sup> and He–Yu<sup>17</sup>, which predict an infinite dilution Fick diffusion coefficient that shows an AARD of approximately 10.8%.

### Infinite dilution Fick diffusion coefficient

A two-step approach to predict the infinite dilution Fick diffusion coefficient of arbitrary CO<sub>2</sub> mixtures on the basis of temperature, pressure (or density) and solute mass is proposed, cf. Fig. 8. In a first step, the self-diffusion coefficient of pure CO<sub>2</sub> is estimated with an entropy scaling approach. Subsequently, this coefficient  $D_{\text{CO}_2}$  is related to the infinite dilution Fick diffusion coefficient by a linear function of molecular solute mass.

First, the Span–Wagner EoS<sup>98</sup>, that is freely available at the NIST Webbook<sup>99</sup>, can be used to estimate the reduced residual entropy  $s^+ = -s^r/R$  of CO<sub>2</sub> at the specified temperature and pressure (or density). The following correlation relates the self-diffusion coefficient of pure CO<sub>2</sub> (in m<sup>2</sup>/s) with the reduced residual entropy

$$D_{\text{CO}_2} = \frac{1}{(\rho N_A)^{1/3} (M_1/(RT))^{1/2}} \cdot \frac{0.5016 \cdot \exp(-0.2031 \cdot s^+)}{(s^+)^{2/3}}, \quad (2)$$

where  $\rho$  the molar density in mol/m<sup>3</sup>,  $N_A$  the Avogadro constant,  $M_1$  the molecular solvent mass in kg/mol,  $R$  the universal gas constant in J/(mol K) and  $T$  the temperature in K. This equation can also be expressed in the following form

$$D_{\text{CO}_2}^+ = D_{\text{CO}_2} \cdot (\rho N_A)^{1/3} (M_1/(RT))^{1/2} \cdot (s^+)^{2/3} = 0.5016 \cdot \exp(-0.2031 \cdot s^+), \quad (3)$$

where  $D_{\text{CO}_2}^+$  is the self-diffusion coefficient of CO<sub>2</sub> scaled according to Bell et al.<sup>100</sup>. The predicted self-diffusion coefficient shows an AARD of ~2.4% to the underlying simulation data depicted in Fig. 8 (left).

Second, present simulations and experimental data indicate that the infinite dilution Fick diffusion coefficient of CO<sub>2</sub> mixtures with a given solute  $D^{x_1 \rightarrow 1}$  is a linear function of the self-diffusion coefficient of pure CO<sub>2</sub> under the studied thermodynamic conditions, cf. Fig. 8 (right). Since the linear equations for each of the solutes pass through the origin, they only differ by the slope, which, in turn, depends on the molecular mass of the solute  $M_2$  by

$$D^{x_1 \rightarrow 1} = 0.1276 \cdot M_2^{-0.6124} \cdot D_{\text{CO}_2}. \quad (4)$$

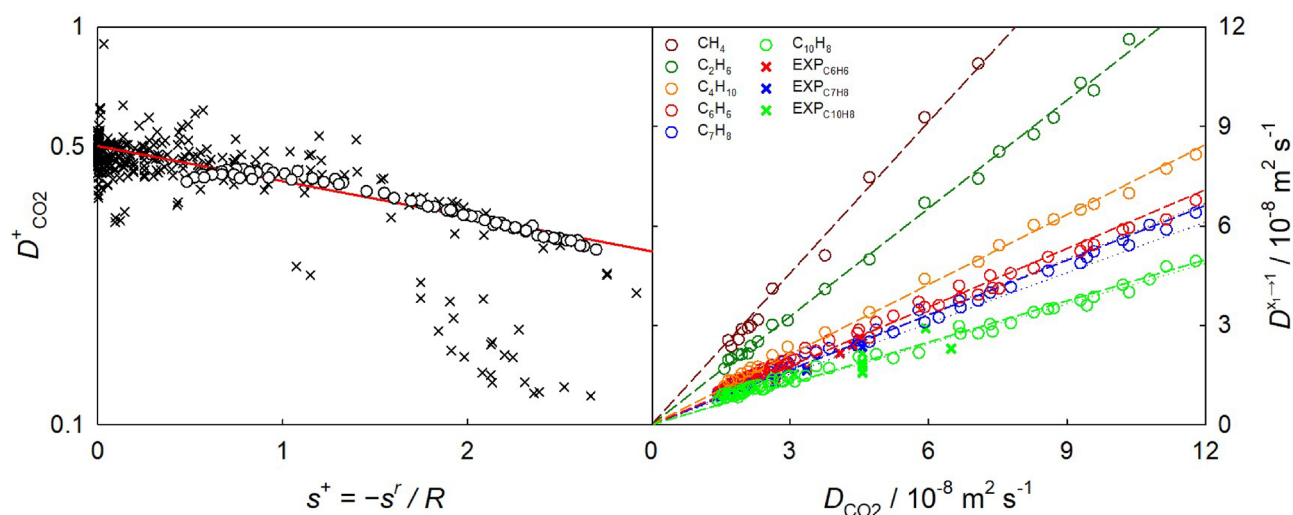


**Figure 8.** Self-diffusion coefficient of pure CO<sub>2</sub> scaled according to Bell et al.<sup>100</sup> over the reduced residual entropy (left). Experimental data for the CO<sub>2</sub> self-diffusion coefficient<sup>103</sup> and simulation data are represented by crosses and circles, respectively. The solid line (red) depicts the present entropy scaling correlation  $D_{\text{CO}_2}^+ = 0.5016 \cdot \exp(-0.2031 \cdot s^+)$ . On the right, the infinite dilution Fick diffusion coefficient of CO<sub>2</sub> mixtures is shown as a function of the self-diffusion coefficient of pure CO<sub>2</sub>. Simulation data for CO<sub>2</sub> mixtures with methane (dark red), ethane (dark green), isobutane (orange), benzene (red), toluene (blue) or naphthalene (green) are represented by open circles. Experimental data for the infinite dilution Fick diffusion coefficient of CO<sub>2</sub> with benzene, toluene and naphthalene (right) are depicted by crosses. Linear regressions of the simulation data are shown by dashed lines.

Hence, using Eqs. (2) and (4) yields the infinite dilution Fick diffusion coefficient of an arbitrary CO<sub>2</sub> mixture at the specified supercritical state point.

The entropy scaling approach by Bell et al.<sup>100</sup> was applied in this work to estimate the self-diffusion coefficient of CO<sub>2</sub>. This particular approach was chosen over Rosenfeld's entropy scaling for liquids<sup>101</sup> and dilute gases<sup>102</sup>, as it was demonstrated to successfully bridge the gap between these two aggregation states<sup>100</sup>.

Figure 8 (left) shows the self-diffusion coefficient  $D_{\text{CO}_2}^+$  scaled according to Bell et al. in combination with the Span-Wagner EoS in comparison with experimental<sup>103</sup> and simulation data for pure CO<sub>2</sub>. The simulation data exhibit an excellent agreement with the experimental data within the reduced residual entropy range  $0.5 < s^+ < 2.8$ , which also validates the employed CO<sub>2</sub> force field model<sup>104</sup>. These data can also be represented in the scaled form proposed by Rosenfeld<sup>101</sup> or by using the entropy-scaling coordinate<sup>105,106</sup> as shown in Fig. S11. Further, other entropy-scaling based correlations to estimate the self-diffusion coefficient of CO<sub>2</sub> on the basis of input data from perturbed-chain polar statistical associating fluid theory (PCP-SAFT)<sup>107,108</sup>, translated-consistent Peng–Robinson (tc-PR) or industrialized PC-SAFT (I-PC-SAFT) EoS<sup>106</sup> can also be used in the first step of the present approach. For instance, the correlation by Dehlouz et al.<sup>106</sup> was recently used to estimate the self-diffusion coefficient of CO<sub>2</sub> and 71 other pure substances.

The proposed two-step prediction approach yields an AARD of 7.4 % to simulation data for all CO<sub>2</sub> mixtures considered in this work, cf. Table S1 and Figs. S6 to S10. The deviation to present experimental data represented in Fig. 9 is 26.8%, which reduces to 11.8% if only the density region  $\rho_{\text{CO}_2} > 400 \text{ kg/m}^3$  is considered.

## Discussion and conclusion

Molecular dynamics simulations were complemented by Taylor dispersion experiments, equations of state and semi-empirical correlations to study the Fick diffusion coefficient of binary CO<sub>2</sub> mixtures in the extended critical region, i.e. in the vicinity of the Widom line. An overview of the available experimental data on the Fick diffusion coefficient of hydrocarbons diluted in scCO<sub>2</sub> was presented together with new experimental data for scCO<sub>2</sub> mixtures with benzene, toluene, n-dodecane and THN along the isobar  $p = 10 \text{ MPa}$ .

It was demonstrated that the thermodynamic factor exhibits a minimum in the proximity of the Widom line. Its magnitude depends on the non-ideality of the mixture, which is related to the size difference between CO<sub>2</sub> and the solute. This non-ideality is a consequence of density fluctuations and the formation of clusters comprising CO<sub>2</sub> molecules around a given solute molecule. The extent of this clustering was quantified by means of the excess coordination number.

The peculiarity of the Fick diffusion coefficient in the near-critical region can be attributed to the presence of a thermodynamic factor minimum. This phenomenon was shown to be particularly pronounced for large solute molecules, like naphthalene or n-dodecane. Consequently, the thermodynamic factor of these mixtures exhibits a more pronounced minimum due to the size disparity leading to stronger clustering.

In the infinite dilution limit, where the thermodynamic factor approaches unity, the Fick diffusion coefficient has a conventional behavior, i.e. it monotonously increases with falling density. As the pressure rises and the system moves further away from the critical region, the thermodynamic factor minimum fades, resulting in a gradual reduction of the peculiar behavior of the Fick diffusion coefficient at finite mole fractions.

A breakdown of the Stokes–Einstein relation was confirmed for the investigated CO<sub>2</sub> mixtures in the proximity of the Widom line. It is very notable for CO<sub>2</sub> mixtures with benzene, toluene or naphthalene, while it is less pronounced e.g. for CO<sub>2</sub> + ethane. The extent of this breakdown can be related to the non-ideality of the mixtures and the strong density fluctuations near the Widom line.

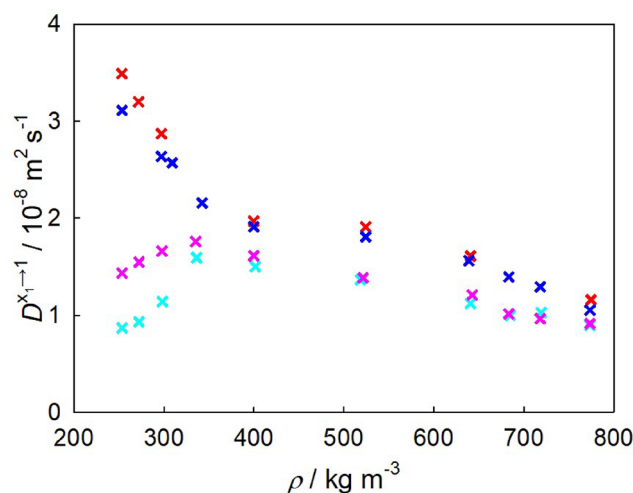


**Figure 9.** Present experimental data for the infinite dilution Fick diffusion coefficient as a function of density. Crosses represent data for CO<sub>2</sub> mixtures with benzene (red), toluene (blue), n-dodecane (pink) and THN (cyan) along the isobar  $p = 10 \text{ MPa}$ .

Eleven semi-empirical correlations to estimate the infinite dilution Fick diffusion coefficient of supercritical CO<sub>2</sub> mixtures were compared to experiments and simulations. Most of these correlations fail to predict the Fick diffusion coefficient under gas-like SCF conditions, characterized by high temperature and low density. The Wilke–Chang and Catchpole–King equations were found to have the best quantitative agreement with simulation data for the studied CO<sub>2</sub> mixtures, with overall AARD of 13.0% and 13.3%, respectively. On the other hand, the best agreement with the present experimental results for CO<sub>2</sub> mixtures with benzene or toluene was observed for the Funazukuri–Wakao and He–Yu correlations, having an average deviation of about 10.8%.

A predictive approach for the infinite dilution Fick diffusion coefficient of CO<sub>2</sub> + hydrocarbon mixtures on the basis of temperature, pressure (or density) and solute mass was proposed. In a first step, entropy scaling was employed to determine the self-diffusion coefficient of pure CO<sub>2</sub>. Subsequently, this coefficient was used to determine the infinite dilution Fick diffusion coefficient of the mixture. These two diffusion coefficients exhibit a linear relationship, where the slope is solely dependent on solute mass. Compared to simulation data, this approach demonstrates an overall AARD of 7.4% for the CO<sub>2</sub> mixtures considered in this work, and hence, a significant improvement over semi-empirical correlations. However, when compared to present experimental data for CO<sub>2</sub> mixtures with benzene, toluene, n-dodecane and THN, it shows an AARD of 26.8%. This can be attributed to the use of simulation data for parameterization, which accurately predict the experimental Fick diffusion coefficient of CO<sub>2</sub> mixtures with aromatics under high-density, liquid-like conditions, but tend to overestimate it under low-density, gas-like conditions.

It should be noted that molecular simulation allows for the determination of the Fick diffusion coefficient for a specified mixture composition. In most experiments, the mixture composition strongly varies until it reaches the infinite dilution limit. In fact, the injected solute in the CO<sub>2</sub> carrier fluid is often injected as a pure fluid at the beginning of the diffusive process. This process thus undergoes the entire composition space. Upon the flow of the mixture through a long capillary, the pulse dilutes itself and the diffusive process approaches infinite dilution asymptotically. Therefore, Taylor dispersion experiments do not occur in the exact infinite dilution limit. When a single Fick diffusion coefficient is assigned to characterize this entire process, which may be slowed down because of the depression of the thermodynamic factor, a too low Fick diffusion coefficient would be identified. This may partially explain the quantitative discrepancies between data from experiments and simulation under low-density, gas-like conditions. Hence, the peculiarity, i.e. the depression of the Fick diffusion coefficient in the near critical region, may be rationalized with the strong composition dependence of this property.

It is expected that the presented two-step approach to predict the infinite dilution Fick diffusion coefficient can be extended to arbitrary CO<sub>2</sub> + hydrocarbon mixtures in the extended critical region. Further studies are needed to assess its applicability to CO<sub>2</sub> mixtures with associating molecular species.

## Methods

### Molecular simulation

All simulations were performed using the open-source program *ms2*<sup>109</sup>. Rigid, united-atom and non-polarizable force fields based on Lennard-Jones (LJ) sites and/or superimposed point dipoles or point quadrupoles were employed. The force fields for the pure substances CO<sub>2</sub><sup>104</sup>, methane<sup>110</sup>, ethane<sup>110</sup>, isobutane<sup>111</sup>, benzene<sup>80</sup>, toluene<sup>80</sup> and naphthalene<sup>112</sup> were parameterized using a combination of quantum chemical calculations, experimental vapor-liquid equilibrium (VLE) data and self-diffusion coefficient measurements in the case of benzene and toluene<sup>80</sup> with a procedure described in Refs.<sup>111,113,114</sup>. For mixtures, LJ parameters for unlike interactions were optimized using combination rules<sup>115</sup> as previously described in Ref.<sup>116</sup>.

Transport properties were sampled with equilibrium molecular dynamics and the Green–Kubo formalism<sup>117,118</sup>. This formalism allows for the simultaneous sampling of intra- and Maxwell–Stefan diffusion coefficients as well as shear viscosity so that it was preferred over non-equilibrium methods. The general Green–Kubo equation relates an arbitrary transport coefficient  $\Xi$  to an integral of a time-correlation function by

$$\Xi = \frac{1}{G} \int_0^\infty dt \langle \dot{\mathbf{A}}(t) \cdot \dot{\mathbf{A}}(0) \rangle. \quad (5)$$

Therein,  $G$  is a transport property-specific factor,  $\mathbf{A}$  the related perturbation and  $\dot{\mathbf{A}}$  its time derivative. The brackets  $\langle \dots \rangle$  denote the ensemble average. The working equations for different diffusion coefficients can be found in Ref.<sup>119</sup>.

The thermodynamic factor can be determined using EoS or excess Gibbs energy models that were fitted to experimental VLE data. Another approach to obtain the thermodynamic factor is through molecular simulation, where chemical potential data or Kirkwood–Buff integrals (KBI) can be utilized. In this study, the thermodynamic factor was calculated based on the microscopic structure of the mixture using Kirkwood–Buff integrals (KBI)  $G_{ij}$ <sup>120</sup>

$$G_{ij} = 4\pi \int_0^\infty dr (g_{ij}(r) - 1) r^2, \quad (6)$$

where  $g_{ij}(r)$  is the radial distribution function. Equation (6) is formulated for the grand canonical ensemble, so that corrections are necessary when applying it in the canonical ensemble<sup>121</sup>. The truncation method proposed by Krüger et al.<sup>122</sup> was employed for this purpose. Moreover, corrections of the radial distribution function based on the method by Ganguly and van der Vegt<sup>123</sup> were employed. The thermodynamic factor was not extrapolated to the thermodynamic limit, as the studied simulation volumes contained a rather large number of molecules ( $N = 5000$ ).

Cluster formation can be characterized by the excess number of solvent molecules surrounding a given solute molecule with respect to the bulk density<sup>64</sup>. The so-called excess coordination number is given by<sup>63</sup>

$$N_{\text{CO}_2}^{\text{ex}} = \rho_{\text{CO}_2} G_{ij}^{\infty}, \quad (7)$$

where  $\rho_{\text{CO}_2}$  is the density of pure CO<sub>2</sub> and  $G_{ij}^{\infty}$  denotes the KBI between carbon dioxide and solute. Further technical simulation details are given in the SI.

**Finite size corrections.** Finite-size corrections for the intra-diffusion coefficients were implemented using the approach by Yeh and Hummer<sup>124</sup>. The magnitude of these corrections varied depending on the density of the system. At high densities, the corrections amounted to approximately 2.4%, while at low densities they increased up to around 10.1% for the sampled infinite dilution Fick diffusion coefficient along the three isobars  $p = 9, 10$  and 12 MPa. Further, two methods were investigated to account for the finite system size in the calculation of the sampled Maxwell–Stefan diffusion coefficient. The first method, proposed by Jamali et al.<sup>125</sup>, involves the thermodynamic factor in the denominator of the diffusion coefficient expression. This method was evaluated alongside additional simulations conducted with varying numbers of molecules (500, 800, 1200, 2500, 5000 and 6000). Four state points were tested for each mixture. Considering the strong decrease of the thermodynamic factor near the Widom line, the correction method by Jamali et al.<sup>125</sup> tended to overestimate the size correction in this region. Therefore, the correction method utilizing progressively larger systems was employed in this study. Thus, the Maxwell–Stefan diffusion coefficient for all studied systems was adjusted by approximately 10% to compensate for the finite system size effects.

## Experiment

**Apparatus.** The Taylor dispersion apparatus used in this work consisted of four modules: a carrier fluid conditioning device, the CO<sub>2</sub> delivery system with a solute injection valve, the air bath thermostat housing the diffusion capillary and a FT-IR detector. A detailed description of the apparatus can be found in Refs.<sup>79,126</sup>, here only the last module is briefly described. The conventional Taylor dispersion setup, which uses a differential refractometer as a detector, is typically suitable for a wide temperature range, but is limited to the low-pressure range below 0.5 MPa. To operate at higher pressures, the introduction of restriction tubes before the refractive index detector is necessary<sup>5</sup>. However, this approach perturbs the diffusion process and can lead to changes of the fluid velocity and distortion of solute dispersion. In contrast, the combination of a Taylor dispersion tube with a FT-IR spectrophotometer and a back pressure regulator allows for decompression of the flow after the detector, without causing any unwanted disturbances. It should be noted that the transmission spectra of scCO<sub>2</sub> exhibit three wide IR transparent regions between 850–1200, 1400–2100 and 2600–3400 cm<sup>-1</sup>, enabling the detection of vibrational modes of solute molecules appearing within these regions.

The Taylor peak was monitored at the outlet of the dispersion tube by a FT-IR spectrophotometer (Jasco FT-IR 4100) with an accuracy of 0.01 cm<sup>-1</sup> and a resolution of 4 cm<sup>-1</sup>. The spectrophotometer was equipped with a high-pressure demountable flow cell (Harrick) with a wall thickness of 150 μm, featuring optical windows made of ZnSe, which allowed for a maximum working pressure of 25 MPa. One of the advantages of the FT-IR detector is its adjustability for an optimal optical path and sample volume. If desired, the optical windows can be made from sapphire, enabling even higher working pressures of up to 50 MPa, surpassing the limitation of 30 MPa in UV high-pressure flow cells<sup>27,43,97</sup>. One additional advantage of the FT-IR detector is its capability to analyze absorption peaks at multiple wavenumbers, which correspond to one (or several) specific types of vibrational modes of a molecule. This allows for a more comprehensive characterization of the sample. The FT-IR data were acquired and processed using Spectra Manager v.2 by Jasco (www.jascoinc.com). Response curves, showing the variation of solute concentration over time, were obtained by monitoring absorbance spectra at specific wavenumbers associated with different molecular vibration modes. The details of the selection of these working wavenumbers, the experimental protocol and the fitting procedure have been reported in Refs.<sup>79,126</sup>.

**Materials.** CO<sub>2</sub> with a certified purity of 99.998 mol% was purchased from Air Liquide in a bottle in its vapor-liquid equilibrium state, i.e., with a nominal pressure  $p = 6.4$  MPa at  $T = 298$  K. Benzene and toluene were purchased from Sigma-Aldrich with a purity of 99.8 mol%, whereas n-dodecane and 1,2,3,4-tetrahydronaphthalene were bought from Acros Organics with 99% and 98% purity, respectively. All solutes were used without further purification.

## Data availability

Excel files containing all data generated or analyzed during this study are included in the Supplementary Information.

Received: 24 July 2023; Accepted: 15 September 2023

Published online: 26 September 2023

## References

1. Brunner, G. Applications of supercritical fluids. *Annu. Rev. Chem. Biomol. Eng.* **1**, 321–342 (2010).
2. Goñi, M. L., Gañán, N. A. & Martini, R. E. Supercritical CO<sub>2</sub>-assisted dyeing and functionalization of polymeric materials: A review of recent advances (2015–2020). *J. CO<sub>2</sub> Util.* **54**, 101760 (2021).
3. Manjare, S. D. & Dhingra, K. Supercritical fluids in separation and purification: A review. *Mater. Sci. Technol.* **2**, 463–484 (2019).
4. Saira Janna, F. & Le-Hussain, F. Effectiveness of modified CO<sub>2</sub> injection at improving oil recovery and CO<sub>2</sub> storage-review and simulations. *Energy Rep.* **6**, 1922–1941 (2020).
5. Cadogan, S. *Diffusion of CO<sub>2</sub> in fluids relevant to carbon capture, utilisation and storage*. Ph.D. thesis, Imperial College London (2015).

6. Li, H., Wilhelmsen, Ø., Lv, Y., Wang, W. & Yan, J. Viscosities, thermal conductivities and diffusion coefficients of CO<sub>2</sub> mixtures: Review of experimental data and theoretical models. *Int. J. Greenh. Gas Control* **5**, 1119–1139 (2011).
7. Funazukuri, T. Concerning the determination and predictive correlation of diffusion coefficients in supercritical fluids and their mixtures. *J. Supercrit. Fluids* **134**, 28–32 (2018).
8. Wilke, C. & Chang, P. Correlation of diffusion coefficients in dilute solutions. *AIChE J.* **1**, 264–270 (1955).
9. Scheibel, E. G. Correspondence. Liquid diffusivities viscosity of gases. *Ind. Eng. Chem.* **46**, 2007–2008 (1954).
10. Tyn, M. T. & Calus, W. F. Diffusion coefficients in dilute binary liquid mixtures. *J. Chem. Eng. Data* **20**, 106–109 (1975).
11. Hayduk, W. & Minhas, B. S. Correlations for prediction of molecular diffusivities in liquids. *Can. J. Chem. Eng.* **60**, 295–299 (1982).
12. Sassi, P. R., Mourier, P., Caude, M. H. & Rosset, R. H. Measurement of diffusion coefficients in supercritical carbon dioxide and correlation with the equation of Wilke and Chang. *Anal. Chem.* **59**, 1164–1170 (1987).
13. Lai, C.-C. & Tan, C.-S. Measurement of molecular diffusion coefficients in supercritical carbon dioxide using a coated capillary column. *Ind. Eng. Chem. Res.* **34**, 674–680 (1995).
14. Funazukuri, T., Kong, C. Y. & Kagei, S. Binary diffusion coefficients in supercritical fluids: Recent progress in measurements and correlations for binary diffusion coefficients. *J. Supercrit. Fluids* **38**, 201–210 (2006).
15. Zêzere, B., Portugal, I., Gomes, J. R. & Silva, C. M. Modeling tracer diffusion coefficients of any type of solutes in polar and non-polar dense solvents. *Materials* **15**, 6416 (2022).
16. Catchpole, O. J. & King, M. B. Measurement and correlation of binary diffusion coefficients in near critical fluids. *Ind. Eng. Chem. Res.* **33**, 1828–1837 (1994).
17. He, C.-H. & Yu, Y.-S. New equation for infinite-dilution diffusion coefficients in supercritical and high-temperature liquid solvents. *Ind. Eng. Chem. Res.* **37**, 3793–3798 (1998).
18. Funazukuri, T., Ishiwata, Y. & Wakao, N. Predictive correlation for binary diffusion coefficients in dense carbon dioxide. *AIChE J.* **38**, 1761–1768 (1992).
19. Kraft, S. & Vogel, F. Estimation of binary diffusion coefficients in supercritical water: Mini review. *Ind. Eng. Chem. Res.* **56**, 4847–4855 (2017).
20. Yang, Y., Stenby, E. H., Shapiro, A. A. & Yan, W. Diffusion coefficients in systems related to reservoir fluids: Available data and evaluation of correlations. *Processes* **10**, 1554 (2022).
21. Liong, K., Wells, P. & Foster, N. Diffusion in supercritical fluids. *J. Supercrit. Fluids* **4**, 91–108 (1991).
22. Bueno, J., Suarez, J. & Medina, I. Experimental binary diffusion coefficients of benzene and derivatives in supercritical carbon dioxide and their comparison with the values from the classic correlations. *Chem. Eng. Sci.* **56**, 4309–4319 (2001).
23. Swaid, I. & Schneider, G. M. Determination of binary diffusion coefficients of benzene and some alkylbenzenes in supercritical CO<sub>2</sub> between 308 and 328 K in the pressure range 80 to 160 bar with supercritical fluid chromatography (SFC). *Ber. Bunsenges. Phys. Chem.* **83**, 969–974 (1979).
24. Umezawa, S. & Nagashima, A. Measurement of the diffusion coefficients of acetone, benzene, and alkane in supercritical CO<sub>2</sub> by the Taylor dispersion method. *J. Supercrit. Fluids* **5**, 242–250 (1992).
25. Levelt Sengers, J., Deiters, U., Klask, U., Swidersky, P. & Schneider, G. Application of the Taylor dispersion method in supercritical fluids. *Int. J. Thermophys.* **14**, 893–922 (1993).
26. Suárez, J. J., Bueno, J. L. & Medina, I. Determination of binary diffusion coefficients of benzene and derivatives in supercritical carbon dioxide. *Chem. Eng. Sci.* **48**, 2419–2427 (1993).
27. Funazukuri, T. & Nishimoto, N. Tracer diffusion coefficients of benzene in dense CO<sub>2</sub> at 313.2 K and 8.5–30 MPa. *Fluid Phase Equilib.* **125**, 235–243 (1996).
28. Funazukuri, T., Kong, C. & Kagei, S. Infinite dilution binary diffusion coefficients of benzene in carbon dioxide by the Taylor dispersion technique at temperatures from 308.15 to 328.15 K and pressures from 6 to 30 MPa. *Int. J. Thermophys.* **22**, 1643–1660 (2001).
29. Filho, C. A., Silva, C. M., Quadri, M. B. & Macedo, E. A. Infinite dilution diffusion coefficients of linalool and benzene in supercritical carbon dioxide. *J. Chem. Eng. Data* **47**, 1351–1354 (2002).
30. Nishiumi, H. & Kubota, T. Fundamental behavior of benzene-CO<sub>2</sub> mutual diffusion coefficients in the critical region of CO<sub>2</sub>. *Fluid Phase Equilib.* **261**, 146–151 (2007).
31. Lin, R. & Tavlarides, L. L. Diffusion coefficients of diesel fuel and surrogate compounds in supercritical carbon dioxide. *J. Supercrit. Fluids* **52**, 47–55 (2010).
32. Santos, C. I., Barros, M. C., Faro, M. P., Shevtsova, V. & Ribeiro, A. C. FTIR as a powerful tool for measurements of diffusion in supercritical carbon dioxide using Taylor dispersion method. *Processes* **10**, 1528 (2022).
33. Bruno, T. J. A supercritical fluid chromatograph for physicochemical studies. *J. Res. Natl. Inst. Stand.* **94**, 105–112 (1989).
34. Knaff, G. & Schlünder, E. Diffusion coefficients of naphthalene and caffeine in supercritical carbon dioxide. *Chem. Eng. Process.* **21**, 101–105 (1987).
35. Lamb, D., Adamy, S., Woo, K. & Jonas, J. Transport and relaxation of naphthalene in supercritical fluids. *J. Phys. Chem.* **93**, 5002–5005 (1989).
36. Akgerman, A., Erkey, C. & Orejuela, M. Limiting diffusion coefficients of heavy molecular weight organic contaminants in supercritical carbon dioxide. *Ind. Eng. Chem. Res.* **35**, 911–917 (1996).
37. Klask, U. Diffusionskoeffizienten in Fluiden: Bestimmung von binären Diffusionskoeffizienten organischer Substanzen in überkritischem Kohlendioxid nach der Taylordispersionsmethode. Ph.D. thesis, Ruhr-Universität Bochum, Germany (1998).
38. Higashi, H., Iwai, Y., Takahashi, Y., Uchida, H. & Arai, Y. Diffusion coefficients of naphthalene and dimethylnaphthalene in supercritical carbon dioxide. *Fluid Phase Equilib.* **144**, 269–278 (1998).
39. Higashi, H., Iwai, Y., Nakamura, Y., Yamamoto, S. & Arai, Y. Correlation of diffusion coefficients for naphthalene and dimethylnaphthalene isomers in supercritical carbon dioxide. *Fluid Phase Equilib.* **166**, 101–110 (1999).
40. Higashi, H., Iwai, Y., Oda, T., Nakamura, Y. & Arai, Y. Concentration dependence of diffusion coefficients for supercritical carbon dioxide + naphthalene system. *Fluid Phase Equilib.* **194**, 1161–1167 (2002).
41. Kong, C. Y., Sone, K., Sako, T., Funazukuri, T. & Kagei, S. Solubility determination of organometallic complexes in supercritical carbon dioxide by chromatographic impulse response method. *Fluid Phase Equilib.* **302**, 347–353 (2011).
42. Tsekhanskaya, Y. V. Solubility of naphthalene in ethylene and carbon dioxide under pressure. *Russ. J. Phys. Chem.* **38**, 1173–1176 (1964).
43. Kong, C. Y., Funazukuri, T. & Kagei, S. Binary diffusion coefficients and retention factors for polar compounds in supercritical carbon dioxide by chromatographic impulse response method. *J. Supercrit. Fluids* **37**, 359–366 (2006).
44. Silva, C. *et al.* Tracer diffusion coefficients of citral and d-limonene in supercritical carbon dioxide. *Fluid Phase Equilib.* **204**, 65–73 (2003).
45. Silva, C. M., Cláudio Filho, A., Quadri, M. B. & Macedo, E. A. Binary diffusion coefficients of  $\alpha$ -pinene and  $\beta$ -pinene in supercritical carbon dioxide. *J. Supercrit. Fluids* **32**, 167–175 (2004).
46. Magalhães, A. L., Lito, P. F., Da Silva, F. A. & Silva, C. M. Simple and accurate correlations for diffusion coefficients of solutes in liquids and supercritical fluids over wide ranges of temperature and density. *J. Supercrit. Fluids* **76**, 94–114 (2013).
47. Saric, D., Guevara-Carrion, G. & Vrabec, J. Thermodynamics of supercritical carbon dioxide mixtures across the Widom line. *Phys. Chem. Chem. Phys.* **24**, 28257–28270 (2022).

48. Raju, M., Banuti, D. T., Ma, P. C. & Ihme, M. Widom lines in binary mixtures of supercritical fluids. *Sci. Rep.* **7**, 1–10 (2017).
49. Raman, A. S., Li, H. & Chiew, Y. Widom line, dynamical crossover, and percolation transition of supercritical oxygen via molecular dynamics simulations. *J. Chem. Phys.* **148**, 014502 (2018).
50. Karalis, K., Ludwig, C. & Niceno, B. Supercritical water anomalies in the vicinity of the Widom line. *Sci. Rep.* **9**, 15731 (2019).
51. Maxim, F. *et al.* Thermodynamics and Dynamics of Supercritical Water Pseudo-Boiling. *Adv. Sci.* **8**, 2002312 (2021).
52. Banuti, D., Raju, M. & Ihme, M. Between supercritical liquids and gases-Reconciling dynamic and thermodynamic state transitions. *J. Supercrit. Fluids* **165**, 104895 (2020).
53. Nishikawa, K. & Tanaka, I. Correlation lengths and density fluctuations in supercritical states of carbon dioxide. *Chem. Phys. Lett.* **244**, 149–152 (1995).
54. Yoshida, N., Matsugami, M., Harano, Y., Nishikawa, K. & Hirata, F. Structure and properties of supercritical water: Experimental and theoretical characterizations. *J. Multidiscip. Sci. J.* **4**, 698–726 (2021).
55. Liu, Z.-Y., Chen, L. & Chen, H. Characterization of dynamic fluctuations of CO<sub>2</sub> fluid parameters at critical regions near the pseudo-critical line. *Phys. Fluids* **34**, 062003 (2022).
56. Guevara-Carrion, G., Ancherbak, S., Mialdun, A., Vrabec, J. & Shevtsova, V. Diffusion of methane in supercritical carbon dioxide across the Widom line. *Sci. Rep.* **9**, 1–14 (2019).
57. Chatwell, R. S., Guevara-Carrion, G., Gaponenko, Y., Shevtsova, V. & Vrabec, J. Diffusion of the carbon dioxide-ethanol mixture in the extended critical region. *Phys. Chem. Chem. Phys.* **23**, 3106–3115 (2021).
58. Gallo, P., Corradini, D. & Rovere, M. Widom line and dynamical crossovers as routes to understand supercritical water. *Nature Commun.* **5**, 1–6 (2014).
59. Imre, A. R., Groniewsky, A., Györke, G., Katona, A. & Velmóvszki, D. Anomalous properties of some fluids with high relevance in energy engineering in their pseudo-critical (Widom) region. *Period. Polytech. Chem. Eng.* **63**, 276–285 (2019).
60. Liao, G. *et al.* Widom line of supercritical CO<sub>2</sub> calculated by equations of state and molecular dynamics simulation. *J. CO<sub>2</sub> Util.* **62**, 102075 (2022).
61. Xu, L. *et al.* Relation between the Widom line and the dynamic crossover in systems with a liquid-liquid phase transition. *Proc. Natl. Acad. Sci. U.S.A.* **102**, 16558–16562 (2005).
62. Stubbs, J. M. Molecular simulations of supercritical fluid systems. *J. Supercrit. Fluids* **108**, 104–122 (2016).
63. Debenedetti, P. G. Clustering in dilute, binary supercritical mixtures: A fluctuation analysis. *Chem. Eng. Sci.* **42**, 2203–2212 (1987).
64. Hamani, A. W. S., Hoang, H., Viet, T. Q. Q., Daridon, J.-L. & Galliero, G. Excess volume, isothermal compressibility, isentropic compressibility and speed of sound of carbon dioxide+ n-heptane binary mixture under pressure up to 70 MPa. II. *Molecular Simul. J. Supercrit. Fluids* **164**, 104890 (2020).
65. Kumar, P. *et al.* Relation between the Widom line and the breakdown of the Stokes–Einstein relation in supercooled water. *Proc. Natl. Acad. Sci. U.S.A.* **104**, 9575–9579 (2007).
66. Montero de Hijes, P., Sanz, E., Joly, L., Valeriani, C. & Caupin, F. Viscosity and self-diffusion of supercooled and stretched water from molecular dynamics simulations. *J. Chem. Phys.* **149**, 094503 (2018).
67. Skarmoutsos, I. & Samios, J. Local intermolecular structure and dynamics in binary supercritical solutions. A molecular dynamics simulation study of methane in carbon dioxide. *J. Mol. Liq.* **125**, 181–186 (2006).
68. Feng, H. *et al.* Molecular dynamics simulation of diffusion and structure of some n-alkanes in near critical and supercritical carbon dioxide at infinite dilution. *J. Phys. Chem. B* **117**, 12525–12534 (2013).
69. Higgoda, U. A., Hellmann, R., Koller, T. M. & Fröba, A. P. Self-diffusion coefficient and viscosity of methane and carbon dioxide via molecular dynamics simulations based on new ab initio-derived force fields. *Fluid Phase Equilib.* **481**, 15–27 (2019).
70. Higgoda, U. A., Kankanamge, C. J., Hellmann, R., Koller, T. M. & Fröba, A. P. Fick diffusion coefficients of binary fluid mixtures consisting of methane, carbon dioxide, and propane via molecular dynamics simulations based on simplified pair-specific ab initio-derived force fields. *Fluid Phase Equilib.* **502**, 112257 (2019).
71. Inomata, H., Saito, S. & Debenedetti, P. G. Molecular dynamics simulation of infinitely dilute solutions of benzene in supercritical CO<sub>2</sub>. *Fluid Phase Equilib.* **116**, 282–288 (1996).
72. Ferreira Coelho, L., Marchut, A., De Oliveira, J. & Balbuena, P. Theoretical studies of energetics and diffusion of aromatic compounds in supercritical carbon dioxide. *Ind. Eng. Chem. Res.* **39**, 227–235 (2000).
73. Zhou, J., Lu, X., Wang, Y. & Shi, J. Molecular dynamics investigation on the infinite dilute diffusion coefficients of organic compounds in supercritical carbon dioxide. *Fluid Phase Equilib.* **172**, 279–291 (2000).
74. Zhou, J., Lu, X., Wang, Y. & Shi, J. A molecular dynamics simulation of infinite dilute diffusion coefficients of benzene and naphthalene in supercritical carbon dioxide. *Chem. J. Chin. Univ.* **21**, 762–765 (2000).
75. Iwai, Y., Higashi, H., Uchida, H. & Arai, Y. Molecular dynamics simulation of diffusion coefficients of naphthalene and 2-naphthol in supercritical carbon dioxide. *Fluid Phase Equilib.* **127**, 251–261 (1997).
76. Higashi, H., Iwai, Y. & Arai, Y. Calculation of self-diffusion and tracer diffusion coefficients near the critical point of carbon dioxide using molecular dynamics simulation. *Ind. Eng. Chem. Res.* **39**, 4567–4570 (2000).
77. Higashi, H., Iwai, Y. & Arai, Y. Comparison of molecular models used in molecular dynamics simulation for tracer diffusion coefficients of naphthalene and dimethylnaphthalene isomers in supercritical carbon dioxide. *Fluid Phase Equilib.* **234**, 51–55 (2005).
78. Yoo, J.-H., Breiher, A., Iwai, Y. & Yoo, K.-P. Diffusion coefficients of supercritical carbon dioxide and its mixtures using molecular dynamic simulations. *Korean J. Chem. Eng.* **29**, 935–940 (2012).
79. Gaponenko, Y., Gousselnikov, V., Santos, C. I. & Shevtsova, V. Near-critical behavior of Fick diffusion coefficient in Taylor dispersion experiments. *Microgravity Sci. Technol.* **31**, 475–486 (2019).
80. Guevara-Carrion, G., Janzen, T., Muñoz-Muñoz, Y. M. & Vrabec, J. Mutual diffusion of binary liquid mixtures containing methanol, ethanol, acetone, benzene, cyclohexane, toluene, and carbon tetrachloride. *J. Chem. Phys.* **144**, 124501 (2016).
81. Antolovic, I., Staubach, J., Stephan, S. & Vrabec, J. Phase equilibria of symmetric Lennard-Jones mixtures and a look at the transport properties near the upper critical solution temperature. *Phys. Chem. Chem. Phys.* **25**, 17627–17638 (2023).
82. Taylor, R. & Kooijman, H. A. Composition derivatives of activity coefficient models (for the estimation of thermodynamic factors in diffusion). *Chem. Eng. Commun.* **102**, 87–106 (1991).
83. Span, R. T. R. E. N. D. *et al.* *Thermodynamic Reference and Engineering Data 5.0* (Lehrstuhl für Thermodynamik, Ruhr-Universität Bochum, 2021).
84. Kim, C.-H., Vimalchand, P. & Donohue, M. D. Vapor-liquid equilibria for binary mixtures of carbon dioxide with benzene, toluene and p-xylene. *Fluid Phase Equilib.* **31**, 299–311 (1986).
85. Janzen, T. *et al.* Mutual diffusion governed by kinetics and thermodynamics in the partially miscible mixture methanol + cyclohexane. *Phys. Chem. Chem. Phys.* **19**, 31856–31873 (2017).
86. Krishna, R. & van Baten, J. M. Describing diffusion in fluid mixtures at elevated pressures by combining the Maxwell–Stefan formulation with an equation of state. *Chem. Eng. Sci.* **153**, 174–187 (2016).
87. Krishna, R. Problems and pitfalls in the use of the Fick formulation for intraparticle diffusion. *Chem. Eng. Sci.* **48**, 845–861 (1993).

88. Kong, C. Y., Withanage, N. R., Funazukuri, T. & Kagei, S. Binary diffusion coefficients and retention factors for long-chain triglycerides in supercritical carbon dioxide by the chromatographic impulse response method. *J. Chem. Eng. Data* **50**, 1635–1640 (2005).
89. Einstein, A. *Investigations on the Theory of the Brownian Movement* (Dover Publications, 1956).
90. Dubey, V., Erimban, S., Indra, S. & Daschakraborty, S. Understanding the origin of the breakdown of the Stokes–Einstein relation in supercooled water at different temperature–pressure conditions. *J. Phys. Chem. B* **123**, 10089–10099 (2019).
91. Dueby, S., Dubey, V., Indra, S. & Daschakraborty, S. Non-monotonic composition dependence of the breakdown of Stokes–Einstein relation for water in aqueous solutions of ethanol and 1-propanol: explanation using translational jump-diffusion approach. *Phys. Chem. Chem. Phys.* **24**, 18738–18750 (2022).
92. Dueby, S. & Daschakraborty, S. Size dependence of solute’s translational jump-diffusion in solvent: Relationship between trapping and jump-diffusion. *Chem. Phys. Lett.* **806**, 140059 (2022).
93. Tsimpanogiannis, I. N., Jamali, S. H., Economou, I. G., Vlught, T. J. & Moulτος, O. A. On the validity of the Stokes–Einstein relation for various water force fields. *Mol. Phys.* **118**, e1702729 (2020).
94. Tsimpanogiannis, I. N., Maity, S., Celebi, A. T. & Moulτος, O. A. Engineering model for predicting the intradiffusion coefficients of hydrogen and oxygen in vapor, liquid, and supercritical water based on molecular dynamics simulations. *J. Chem. Eng. Data* **66**, 3226–3244 (2021).
95. Tsimpanogiannis, I. N. & Moulτος, O. A. Is Stokes–Einstein relation valid for the description of intra-diffusivity of hydrogen and oxygen in liquid water?. *Fluid Phase Equilib.* **563**, 113568 (2022).
96. Dubey, V. & Daschakraborty, S. Breakdown of the Stokes–Einstein relation in supercooled water/methanol binary mixtures: Explanation using the translational jump-diffusion approach. *J. Phys. Chem. B* **124**, 10398–10408 (2020).
97. Funazukuri, T., Kong, C. & Kagei, S. Binary diffusion coefficients of acetone in carbon dioxide at 308.2 and 313.2 K in the pressure range from 7.9 to 40 MPa. *Int. J. Thermophys.* **21**, 651–669 (2000).
98. Span, R. & Wagner, W. A new equation of state for carbon dioxide covering the fluid region from the triple-point temperature to 1100 K at pressures up to 800 MPa. *J. Phys. Chem. Ref. Data* **25**, 1509–1596 (1996).
99. Huber, M. L., Lemmon, E. W., Bell, I. H. & McLinden, M. O. The nist reprop database for highly accurate properties of industrially important fluids. *Ind. Eng. Chem. Res.* **61**, 15449–15472 (2022).
100. Bell, I. H., Messerly, R., Thol, M., Costigliola, L. & Dyrre, J. C. Modified entropy scaling of the transport properties of the Lennard-Jones fluid. *J. Phys. Chem. B* **123**, 6345–6363 (2019).
101. Rosenfeld, Y. Relation between the transport coefficients and the internal entropy of simple systems. *Phys. Rev. A* **15**, 2545 (1977).
102. Rosenfeld, Y. A quasi-universal scaling law for atomic transport in simple fluids. *J. Phys.: Condens. Matter* **11**, 5415 (1999).
103. Suárez-Iglesias, O., Medina, I., Sanz, M. & D. I. A., Pizarro, C., Bueno, J. L. Self-diffusion in molecular fluids and noble gases: Available data. *J. Chem. Eng. Data* **60**, 2757–2817 (2015).
104. Merker, T., Engin, C., Vrabec, J. & Hasse, H. Molecular model for carbon dioxide optimized to vapor-liquid equilibria. *J. Chem. Phys.* **132**, 234512 (2010).
105. Dehlou, A., Privat, R., Galliero, G., Bonnissel, M. & Jaubert, J.-N. Revisiting the entropy-scaling concept for shear-viscosity estimation from Cubic and SAFT equations of state: application to pure fluids in gas, liquid and supercritical states. *Ind. Eng. Chem. Res.* **60**, 12719–12739 (2021).
106. Dehlou, A., Jaubert, J.-N., Galliero, G., Bonnissel, M. & Privat, R. Entropy scaling-based correlation for estimating the self-diffusion coefficients of pure fluids. *Ind. Eng. Chem. Res.* **61**, 14033–14050 (2022).
107. Hopp, M., Mele, J. & Gross, J. Self-diffusion coefficients from entropy scaling using the pc-p-saft equation of state. *Ind. Eng. Chem. Res.* **57**, 12942–12950 (2018).
108. Zmpitas, J. & Gross, J. Modified Stokes–Einstein equation for molecular self-diffusion based on entropy scaling. *Ind. Eng. Chem. Res.* **60**, 4453–4459 (2021).
109. Fingerhut, R. *et al.* ms2: A molecular simulation tool for thermodynamic properties, release 4.0. *Comp. Phys. Commun.* **262**, 107860 (2021).
110. Vrabec, J., Stoll, J. & Hasse, H. A set of molecular models for symmetric quadrupolar fluids. *J. Phys. Chem. B* **105**, 12126–12133 (2001).
111. Eckl, B., Vrabec, J. & Hasse, H. Set of molecular models based on quantum mechanical ab initio calculations and thermodynamic data. *J. Phys. Chem. B* **112**, 12710–12721 (2008).
112. Stephan, S., Horsch, M. T., Vrabec, J. & Hasse, H. MolMod—an open access database of force fields for molecular simulations of fluids. *Mol. Simul.* **45**, 806–814 (2019).
113. Merker, T., Vrabec, J. & Hasse, H. Engineering molecular models: Efficient parameterization procedure and cyclohexanol as case study. *Soft Mater.* **10**, 3–25 (2012).
114. Muñoz-Muñoz, Y. M., Hsieh, C.-M. & Vrabec, J. Understanding the differing fluid phase behavior of cyclohexane+ benzene and their hydroxylated or aminated forms. *J. Phys. Chem. B* **121**, 5374–5384 (2017).
115. Schnabel, T., Vrabec, J. & Hasse, H. Unlike Lennard–Jones parameters for vapor-liquid equilibria. *J. Mol. Liq.* **135**, 170–178 (2007).
116. Vrabec, J., Huang, Y.-L. & Hasse, H. Molecular models for 267 binary mixtures validated by vapor-liquid equilibria: A systematic approach. *Fluid Phase Equilib.* **279**, 120–135 (2009).
117. Green, M. S. Markoff random processes and the statistical mechanics of time-dependent phenomena. II. Irreversible processes in fluids. *J. Chem. Phys.* **22**, 398–414 (1954).
118. Kubo, R. Statistical-mechanical theory of irreversible processes I. General theory and simple applications to magnetic and conduction problems. *J. Phys. Soc. Jpn.* **12**, 570–586 (1957).
119. Muñoz-Muñoz, Y. M., Guevara-Carrion, G. & Vrabec, J. Molecular insight into the liquid propan-2-ol+ water mixture. *J. Phys. Chem. B* **122**, 8718–8729 (2018).
120. Kirkwood, J. G. & Buff, F. P. The statistical mechanical theory of solutions. I. *J. Chem. Phys.* **19**, 774–777 (1951).
121. Milzetti, J., Nayar, D. & van der Vegt, N. F. Convergence of Kirkwood–Buff integrals of ideal and nonideal aqueous solutions using molecular dynamics simulations. *J. Phys. Chem. B* **122**, 5515–5526 (2018).
122. Krüger, P. *et al.* Kirkwood–Buff integrals for finite volumes. *J. Phys. Chem. Lett.* **4**, 235–238 (2013).
123. Ganguly, P. & van der Vegt, N. F. A. Convergence of sampling Kirkwood–Buff integrals of aqueous solutions with molecular dynamics simulations. *J. Chem. Theory Comput.* **9**, 1347–1355 (2013).
124. Yeh, I. C. & Hummer, G. System-size dependence of diffusion coefficients and viscosities from molecular dynamics simulations with periodic boundary conditions. *J. Phys. Chem. B* **108**, 15873–15879 (2004).
125. Jamali, S. H. *et al.* Finite-size effects of binary mutual diffusion coefficients from molecular dynamics. *J. Chem. Theory Comput.* **14**, 2667–2677 (2018).
126. Ancherbak, S., Santos, C., Legros, J., Mialdun, A. & Shevtsova, V. Development of a high-pressure set-up for measurements of binary diffusion coefficients in supercritical carbon dioxide. *Eur. Phys. J. E* **39**, 111 (2016).

## Acknowledgements

D. S. gratefully acknowledges the support by the Konrad-Adenauer-Stiftung e.V. This work was funded by the Deutsche Forschungsgemeinschaft (DFG) under the grant VR 6/11 and by BMBF under the Grant “16ME0613” WindHPC and conducted under the auspices of the Boltzmann-Zuse Society of Computational Molecular Engineering (BZS). Molecular dynamics simulations were performed either on the Cray CS500 system *Noctua* at the Paderborn Center for Parallel Computing (PC<sup>2</sup>) or on the HPE Apollo system *Hawk* at the High-Performance Computing Center Stuttgart (HLRS) contributing to the project MMHBF2. V.S. gratefully acknowledges the support by KK-2023/00016 - M4SMART (Research Group Program) and PRE-2019-1-0202 of the Basque Government.

## Author contributions

V.S., J.V. and G.G.C. formulated the research questions, D.S. and G.G.C. performed the simulation runs and calculations with the predictive equations, Y.G. conducted the experiments. D.S., G.G.C., V.S. and J.V. wrote the manuscript. All authors analyzed the results and reviewed the manuscript.

## Funding

Open Access funding enabled and organized by Projekt DEAL.

## Competing interests

The authors declare no competing interests.

## Additional information

**Supplementary Information** The online version contains supplementary material available at <https://doi.org/10.1038/s41598-023-42892-7>.

**Correspondence** and requests for materials should be addressed to J.V.

**Reprints and permissions information** is available at [www.nature.com/reprints](http://www.nature.com/reprints).

**Publisher's note** Springer Nature remains neutral with regard to jurisdictional claims in published maps and institutional affiliations.



**Open Access** This article is licensed under a Creative Commons Attribution 4.0 International License, which permits use, sharing, adaptation, distribution and reproduction in any medium or format, as long as you give appropriate credit to the original author(s) and the source, provide a link to the Creative Commons licence, and indicate if changes were made. The images or other third party material in this article are included in the article's Creative Commons licence, unless indicated otherwise in a credit line to the material. If material is not included in the article's Creative Commons licence and your intended use is not permitted by statutory regulation or exceeds the permitted use, you will need to obtain permission directly from the copyright holder. To view a copy of this licence, visit <http://creativecommons.org/licenses/by/4.0/>.

© The Author(s) 2023